



23 European Conference on Fracture – ECF23

An Industrial Approach to High Strain Rate Testing

Chiamaka Emilia Ikenna-Uzodike^{a,b,*}, Yin Jin Janin^b, Marius Gintalas^c, Wei Wen^a,
Artūras Tadžijevas^d, Pedro E.J. Rivera-Diaz-del-Castillo^a

^a*School of Engineering, Lancaster University, Lancaster LA1 4YW, United Kingdom*

^b*National Structural Integrity Center (NSIRC), The Welding Institute (TWI) Ltd, Great Abington, Cambridge, CB21 6AL, United Kingdom*

^c*Brunel University, Kingston Ln, London, Uxbridge UB8 3PH United Kingdom*

^d*Marine Research Institute, Mechanics and Marine Engineering Laboratory, Klaipėda University, LT-92294 Klaipėda, Lithuania*

Abstract

Some industrial applications require properties of materials to be determined to evaluate components' safety in the event of loading and impact. Understanding the behaviour of materials subjected to extreme dynamic loading will aid in enhancing their design. This work is based on developing methods to appraise high loading rate measurements. Different approaches to quantify material properties such as finite element method (FEM), instrumented Charpy testing, and impact testing using servo-hydraulic testing machines are included. Testing is performed at various loading rates, extending existing quasi-static fracture toughness determination to higher loading rates, and accounting for strain-rate dependent properties. The high loading rate servo-hydraulic test machine located at TWI, Cambridge has the capacity to test up to a displacement rate of 20 m/s. The force, displacement, and time parameters are captured by Digital Image Correlation (DIC), which improves the accuracy of the results obtained from experiments. Moreover, the underlying plasticity theory to capture the influence of the strain rate is presented, along with damage constants for FEM calculations adopting the Johnson-Cook model. In addition to the Johnson-Cook approach, analytical solutions using dislocation evolution theory were applied which features the effects of phonon drag and dynamic recovery coefficient in body-centered cubic materials of which X65 grade steel was applied. Also, a deep learning framework was built to predict the tensile curves when given specific test conditions and sample specifications. It was found that high strain rate tests lead to local change at the crack tip which increases plasticity and reduces fracture toughness with single-edged notched three-point bend specimen. The yield strength of the material increased with loading rates during tensile testing leading to a ductile to brittle transition of metals. These strategies were used to establish a revised approach for high strain rate testing and predicting stress-strain curves with a machine learning algorithm.

© 2022 The Authors. Published by Elsevier B.V.

This is an open access article under the CC BY-NC-ND license (<https://creativecommons.org/licenses/by-nc-nd/4.0>)

Peer-review under responsibility of the scientific committee of the 23 European Conference on Fracture – ECF23

Keywords: Dynamic loading; Plasticity; Fracture toughness

* Corresponding author. Tel.: +44 7466341718

E-mail address: c.mbanusi@lancaster.ac.uk

1. Introduction

High strain rate testing is usually analysed using the procedures for quasi-static testing. Its analysis is limited due to the testing standardisation not being sufficient for dynamic testing and difficulty in experimental measurements due to high loading rates and the presence of oscillations in the measured data. The high loading rate testing plays an important roles in high impact characterisation of material properties and application to the assessment of structural integrity. The high loading rate assessment would be used to determine the fitness-for-service purpose, damage tolerance in design, and quality assurance of metallic structures, such as the oil and gas piping, nuclear pressure vessels and tanks, ships, automotive, armour design and aircraft structures. Therefore, mechanical testing at high strain rates have been a very important research area in characterisation of metallic materials for engineering applications.

The force-displacement plots and stress-strain curves are the most important parameters utilised for material characterisation such as the yield stress, the ultimate tensile strength (UTS), elongation and fracture toughness of the materials. The deformation of ductile materials comprises of the elastic and plastic deformations, of which the UTS are assessed within the plastic zone. Due to the importance of plasticity in characterising ductile material properties, plastic deformation has gained a wide interest in research as a result of its complexity. Many approaches [Banerjee et al. \(2015\)](#), [Klopp et al. \(1985\)](#) have been used to describe plastic deformation in materials. The well-know Johnson-Cook model [Johnson et al. \(1983\)](#) for damage and ductile evolution, and failure prediction in engineering materials was applied in this work to describe the plastic deformation and the parameters were used in modelling the finite element analysis in ABAQUS dynamic explicit model.

To characterise material properties at high strain rates, most researchers [Kolsky et al. \(1949\)](#) employed the popular Hopkinson's pressure bar experimental methods due to its cost-effectiveness and simplicity. [Al-Mousawi et al. \(1997\)](#) outlined the procedures to carry out the split Hopkinson pressure bar (SHPB) experiment which they find limitations with the based theory of one-dimensional wave propagation SHPB depends on. In this work, other methods for high strain rate testing were explored such as drop weight tests, instrumented Charpy tests, and the use of an Instron machine adopting the digital image correlation methods for high strain rate tests. The DIC utilised a high-speed camera to capture continuously the stages of deformation and were analysed with GOM software to determine the stress-strain curves for material characterisation.

Nomenclature

ISO	International Organization for Standardization	DIC	Digital image correlation
EDM	Electrical Discharge Machining	TWI	The Welding Institute
FEM	Finite Element Method	SHPB	Split Hopkinson pressure bar
FEA	Finite Element Analysis	API	American Petroleum Institute
JC	Johnson-Cook	BS	British Standard
BCC	Body cubic centered	TEM	Transmission electron microscopy
MLP	Multilayer Perceptron	ASTM	American society for testing and materials

2. Analytical Method

2.1. Thermostatistical model - Evolution of dislocation density

To obtain the flow stress during plastic deformation through physical mechanisms, an irreversible thermodynamic approach of [Huang et al. \(2009\)](#) for polycrystalline materials was employed. [Hirsch et al. \(2006\)](#) found through TEM micrographs that the dislocation structures of materials differ from quasi-static strain rates to high strain rates. High strain rate testing has been associated with strong oscillations during plastic deformation in metals due to significant inertia effects, thus, plastic deformation at high strain rates could be assessed by the theory of dislocation evolution as

modelled by Huang et al. (2009) and Galindo-Nava et al. (2012) for BCC metals. This model was developed for FCC metals and has also been applied for BCC metals. The main theory of this model is based on irreversible thermodynamics which is based on the first and second laws of thermodynamics with the entropic analysis incorporating three irreversible processes including dislocation generation, dislocation annihilation, and dislocation glide. The thermodynamical description reduces to the classical Kocks-Mecking model Kocks et al. (2003) which has been used widely to describe the mechanical behaviour of materials during plastic deformation Huang et al. (2009). This theory importantly takes into account the interaction between the generation and annihilation (dynamic recovery) of dislocation at different strain rates, of which the corresponding evolution of average dislocation density emerge from the description of entropy generation as:

$$\frac{d\rho}{dt} = \frac{\tau_f \dot{\gamma}}{2E} - \frac{d\rho^-}{dt}. \quad (1)$$

Where τ_f is the dislocation glide frictional, $\dot{\gamma}$ is the shear strain rate, E is the dislocation potential energy per unit length, and $d\rho^-$ is the dislocation length per unit volume at time interval of dt . Dislocation annihilation was further explored and considered other factors like the dislocation cross-slip, activation energy and friction stress to modify Equation 1 and rewrite the dislocation evolution as;

$$\frac{d\rho}{d\gamma} = \frac{\tau_0}{\mu b^2} \left[1 - \exp\left(-\frac{\dot{\gamma}}{\dot{\gamma}_0}\right) \right] + \frac{\beta}{b} \sqrt{\rho} - \frac{\mu b^4}{8\pi x V} \frac{\nu_D}{\dot{\gamma}} \times \exp\left[-A \ln\left(\frac{\mu b^4}{16\pi x V} \frac{\nu_D}{\dot{\gamma}}\right) + \frac{\tau V}{\mu b^3}\right] \rho. \quad (2)$$

where μ is the shear modulus, b is the magnitude of the Burgers vector, $\dot{\gamma}$ is shear strain rate, β is a constant accounting for the interaction between dislocations, ν_D is Debye frequency, V is the activation volume, x is stacking fault energy, τ is the shear stress, τ_0 , $\dot{\gamma}_0$, and A are fitting parameters. True normal stress and strain were derived from $\sigma = M\tau$ and $\varepsilon = \gamma/M$ respectively, where M is the Taylor factor.

By the same model, we analytically express the flow stress σ proposed by Kocks et al. (2003) for plastic deformation,

$$\sigma = \sigma_0 + \alpha M \mu b \sqrt{\rho}. \quad (3)$$

where μ is the shear modulus and b is the magnitude of the Burgers vector. The evolution of the average dislocation density ρ was obtained using the expression in Equation 2, with initial density ρ_0 taken into consideration before deformation. By applying this model in BCC metals, it was found that the term describing the dislocations interaction, α values, which is constant in FCC metals like copper changes with strain rates in BCC metals as expressed by Lavrentev (1980) to give a good correlation with the experimental data shown in Fig. 5.

2.2. Johnson-Cook Model

To quantify the relationship between stress and strain at high strain rates, a model is used to characterise this relationship known as the Johnson-Cook equation. The Johnson-Cook (JC) model proposed by Johnson and Cook Johnson et al. (1983) expressed in Equation 4, was used to predict the plastic deformation with the experimentally obtained constants A , B , n and c . The equation defines the flow stress behaviour in terms of strain hardening, strain rate dependence and an effective temperature component. It was used to predict the flow stress, and the material constants were obtained through un-notched, notched round tensile tests, and high strain tensile tests. These are embodied in the three terms on the right-hand side of Equation 4:

$$\sigma = (A + B\varepsilon^n) \left(1 + C \ln \frac{\dot{\varepsilon}}{\dot{\varepsilon}_0} \right) \left(1 - \frac{T - T_r}{T_m - T_r} \right)^m \quad (4)$$

where A , B , n , and C are material constants representing the yield stress at reference conditions, a strain hardening constant, a strain hardening coefficient, and a strengthening coefficient of strain rate, respectively. σ is the effective stress, ε is the equivalent plastic strain, $\dot{\varepsilon}$ is the strain rate, $\dot{\varepsilon}_0$ is the reference strain rate taken as 1 s^{-1} . In this study, the deformation temperature T , and the reference temperature, T_R , are considered at room temperature 22°C , hence, the thermal softening coefficient m is equal to 1, where T_m is the melting temperature. True stress and strain values

derived from experimental data in quasi-static tensile tests were used to derive the strain hardening components, B and n . A was taken as the 0.2 % yield stress of the material at quasi-static testing. With the values of A and an assumed reference strain rate of 1 s^{-1} , a plot of the natural logarithm of $(\sigma - A)$ against the natural logarithm of the true strain (ϵ) was obtained. The value of the slope reveals n , while the intercept is utilized to determine B . The stress-strain data from different strain rates were used to obtain the parameter C parameter as a rate-dependent constant. Regression, as well as optimisation methods, were used for this analysis.

2.3. Johnson-Cook damage material model

The expression of the JC damage model is given as;

$$\epsilon_f = [D_1 + D_2 \exp(D_3 \sigma^*)][1 + D_4 \ln(\dot{\epsilon}_p^*)][1 + D_5 T^*] \quad (5)$$

where ϵ_f is the equivalent strain at failure, $D_1 - D_5$ are damage coefficients, $\sigma^* = \frac{\sigma_m}{\sigma_{eq}}$ is the triaxiality factor, σ_m is the mean stress, σ_{eq} is the equivalent stress, $\dot{\epsilon}_p^* = \frac{\dot{\epsilon}_p}{\dot{\epsilon}_0}$, $\dot{\epsilon}_p$ is the plastic strain rate, $\dot{\epsilon}_0$ is the reference strain rate, $T^* = \frac{T - T_R}{T_m - T_R}$, where T is the deformation temperature, T_R is the reference temperature, and T_m is the melting temperature.

To determine D_1 , D_2 , and D_3 , the stress triaxiality defined as mean stress divided by equivalent stress was obtained using the notched and un-notched round tensile specimens. The value of stress triaxiality for the smooth round specimen is $1/3$, while the Bridgman analytical model stated in Equation 6 was used to derive the triaxiality of notched samples. The Levenberg-Marquardt algorithm in MATLAB was used to fit the parameters of D_1 , D_2 , and D_3 from the plot of fracture strain against triaxiality.

$$\sigma^* = \frac{1}{3} + \ln\left(1 + \frac{a_0}{2R_0}\right) \quad (6)$$

where a_0 is the radius of the notched specimen at the initial cross-sectional area and R_0 is the specimen notch radius. The JC parameters obtained from the experimental data were presented in Table 1, and it was applied in FEM analysis to model the plasticity and dynamic failure model in Abaqus/Explicit.

Table 1. Johnson-Cook ductile and damage variables

T(k)	A (MPa)	B (MPa)	n	c	m	D_1	D_2	D_3	D_4	D_5
295	482	1041	0.7996	0.0319	1	-2.5686	2.7045	0.005	0.0031	0

3. Experimental Analysis

3.1. X65 Grade Steel material

All specimens used for this study were cut from the API 5L X65 alloy steel with chemical composition in Table 2, and were prepared and tested at room temperature at different strain rates ranging from 10^{-3} to 10^2 s^{-1} . The microstructure of the X65 material shown in Fig. 1a shows banding of ferrite-rich and pearlite-rich areas interconnected with pearlitic colonies, and was obtained under optical microscope. Due to the colony of pearlite comprising the ferrite which is the crystal structure of BCC and cementite (Fe_3C), X65 material in this study was classified as a BCC crystal, and was considered in the thermostatistical model.

Tensile tests were performed following the BS standard specification ISO 6892 (2019), drop weight tests were performed with no specific standard, and instrumented Charpy test ISO 12135 (2016), ASTM E1820 (2020), to obtain the force-displacement and stress-strain curves for material characterisation of the ductile and damage parameters of Johnson-Cook model. Three different types of testing were conducted to obtain the desired results necessary for the JC model in computational analysis and machine learning algorithm.

Table 2. Chemical composition of X65 grade steel in (wt%)

C	Mn	Si	Ni	Cr	Mo	V	Cu	Fe
0.1	1.13	0.25	0.11	0.14	0.1	0.06	0.16	remaining

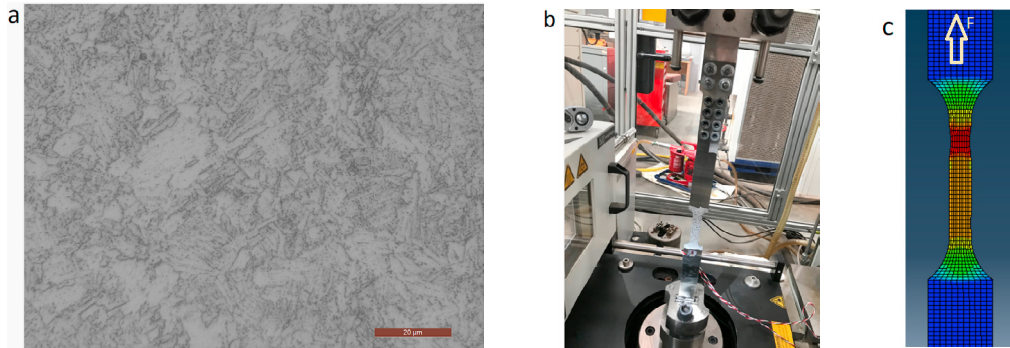


Fig. 1. (a) optical image of X65 grade steel; (b) High strain rate tensile test set-up; (c) FEA model for High strain rate tensile test.

3.2. Quasi-Static Testing

The tensile tests were conducted to derive material properties and parameters required in JC model for ductile damage constants in ABAQUS/Explicit simulations. Based on the need to obtain the JC constants, four samples, made up of round un-notched specimens and round notched specimens as seen in Fig. 2a, were tested at a quasi-static strain rate of 10^{-4} s^{-1} under ambient temperature with a universal testing machine. The tests were to determine the material properties of X65 grade steel such as the 0.2 % yield stress taken as the *A* constant in the JC model, ultimate tensile strength, modulus of elasticity and elongation. Also, the tests on notched samples Fig. 2a with different radii were utilised to obtain the stress triaxiality that aid to obtain the damage parameters D_1 , D_2 , and D_3 .

3.3. High Strain Rate Testing

When dynamic deformation is being discussed, it is important to notice that the statement ‘strain rate’ is a critical parameter and not the velocity of deformation. The rate dependence on the material deformation is considered when trying to determine the rate effect on material properties of the materials. High strain rate tensile testing was designed

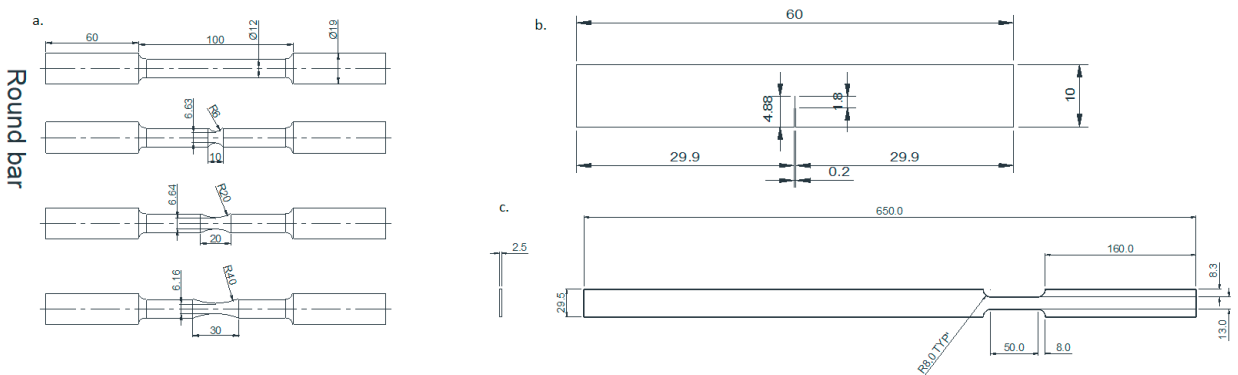


Fig. 2. (a) Round un-notched and notched; (b) Three-point bend specimen Electrical Discharge Machining (EDM) notched and fatigue pre-cracked; (c) Flat high strain rate tensile test specimen. All dimensions in mm with surface texture R_a 1.6 μm .

to derive the rate-dependent constants to be applied in the JC plasticity and damage models. Strain rate is obtained from specimen geometry and experimental data.

The testing machine used for the high rate tensile testing is the B1003 INSTRON VHS under displacement mode with the guide of ISO 26203 (2011) testing standard. The machine in Fig. 1c comprises a 4-column frame, a high-rate actuator with a maximum velocity of 20 m/s, a hydraulic manifold, a hydraulic package, a tool set, a digital controller capable of running both static and dynamic tests. Also, it has a high-performance personal computer for data acquisition, system software and test fixture of which the static unit is mounted on the load frame and dynamic to the piston. The machine has the capacity to hold between 0.5 to 4 mm in thickness. It has a bending fixture which allows impact bend test on a 3-point bend specimen similar to Charpy, with the striker of up to 20 m/s rated velocity mounted to piston.

The initial condition for these test includes setting the actuator velocity, securing the test specimen firmly at the grip region at the allowed distance, choice of allowable gauge length and thickness, type of specimen to fit in (in this case flat specimen), attaching the strain gauges to record along side with the load acquisition system. Also, dual camera is set up for capturing the testing using the Digital Image Correlation (DIC) to record the readings. The outputs expected are the stress from force transducer, strain calculated from the DIC data, Ram displacement and test time. The design of the dog-bone specimen for high strain rate tensile testing was carefully done to accommodate the machine capacity and avoid the specimen from snapping at the grip end. The strain rates were obtained from the division of the maximum velocity with the extensometer gauge length calculated using the equation, $\dot{\epsilon} = \frac{V_{max}}{L}$, where V_{max} is the highest velocity of the machine which was 20 m/s and the L is the extensometer gauge length taken as 25 mm, with 800 s^{-1} being the maximum rate the machine can accommodate.

From Fig. 1b, it can be seen that the specimen was covered with a speckle pattern to aid continuous camera capture during the experiment. The speckle pattern was applied using canned spray paint on the polished surface of the X65 alloy. The strain gauges were placed on both the front and back surfaces during testing which measures the localised strain measurement. To obtain the full strain field for the dynamic testing, DIC technique was utilized. Two sets of images were obtained from the two cameras at separate angles. Calibrations were done on the system to determine the event space of which the value was used to correlate the images in order to derive the surface deformation and strain. The captured images were uploaded in a new project in GOM correlate, a surface component was applied and an extensometer was constructed across the fractured surfaces. The high strain rate tensile test was conducted to obtain the strain rate effects constants in the JC model and to investigate the behaviour of steel at increased loading rates.

3.4. Instrumented Charpy Testing

Impact loading was applied to obtain the desired high strain rate by dropping the pendulum from a fixed height to fracture the notched three-point bend sample ($10 \times 10 \times 60$) mm shown in Fig. 2b. The testing was done in accordance with the BS EN ISO 14556 standard on EDM notched and fatigue pre-cracked samples. Some of the samples were fatigue pre-cracked to investigate the behaviour of a notch and sharp crack within the dynamic testing conditions. The resulting curves from both samples show that the type of crack has little effect on the material behaviour with the crack length being the most important factor to put into consideration. This was also confirmed using the machine learning algorithm to estimate the features that determine the different types of curves obtained from the experimental analysis. The impact drop weight tests were also performed on the specimen with different notches of crack length to width ratio (a_0/W) of 0.2 and 0.5. Different weight values were employed to determine the crack propagation at high impact. These tests were performed according to BS ISO 12135 (2016) and ASTM E 1820.

4. Computational Analysis

4.1. Finite Element Method

For FEA, the implemented JC model was utilised to model the deformation at high strain rates. The JC parameters are of two parts, the ductile and the damage constants. These values were established from experimental results such as the tensile tests for the yield strength, notched tensile test for the stress triaxiality parameter, flat specimen high strain rate testing for the strain-based parameter. All tests were conducted at room temperature.

Fracture strain, ϵ_f , which is the maximum strain a material can withstand prior to fracture, was obtained from the experimental data. The point at which fracture strain was obtained assumes that crack initiation sets in at that point and propagate until fracture. Materials are known to fracture in two ways; brittle and ductile tearing (shows plastic deformation before fracture).

4.2. Machine Learning Model

An artificial intelligent approach was considered to predict the stress-strain curve, and a machine learning algorithm was adopted to predict the curve from known features. In order to apply a consistent dataset for the machine learning, the force-displacement curves were converted to stress-strain curves using the specimen geometry and angle of deformation. Twenty-eight experimental datasets were utilised, and the training and testing data were randomly selected to the ratio of 3:1 respectively. The data processing was done with seven features taken as input which include the type of test, strain rates, specimen geometry, impact mass, initial diameter, temperature and initial cross-section area of the samples. The stress was the output represented with a set of 200 data points in each dataset to generate the curves. The MLP Regressor architecture by Pedregosa et al. (2011) was employed in machine learning to model the stress-strain curve. This architecture has the capacity to model non-linear models, and the trained curves are presented in Fig. 3 for all specimen samples.

5. Discussion

The results of the high strain rate tensile tests were shown in Fig. 5. This shows that, the oscillations are reduced at lower rates and increase significantly as the rate increases to a displacement rate of 10 m/s and 15 m/s. The results obtained from instrumented Charpy test and impact drop weight test show very significant oscillations masking the true path of the curve. Through machine learning, it could be seen that the type of tests determines the shape of the curve: Round tensile is the basic strain curve and flat specimen tensile test at high strain rates gives oscillation. Another factor is the strain rates as this affects the curve shape and gives higher yield strength at higher strain rates.

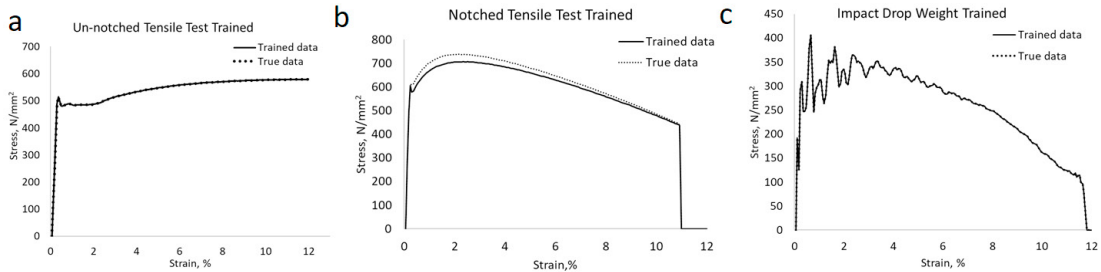


Fig. 3. (a) Training data round un-notched sample; (b) Training data round notched sample; (c) Training data impact drop weight test.

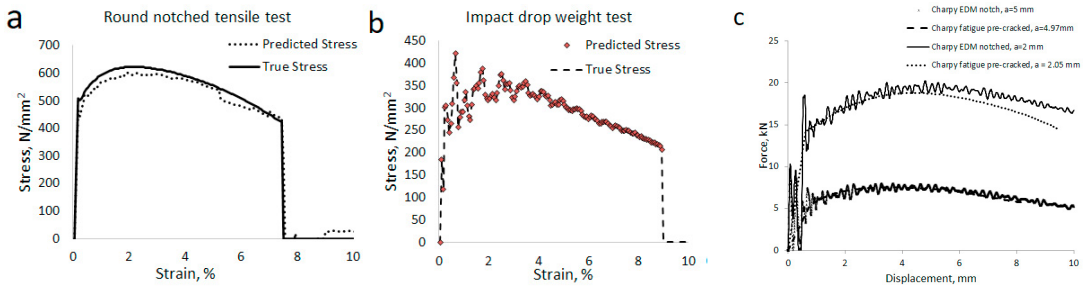


Fig. 4. (a) Testing data round notched sample; (b) Testing data impact drop weight; (c) Comparison of fatigue pre-cracked and EDM notched sample results.

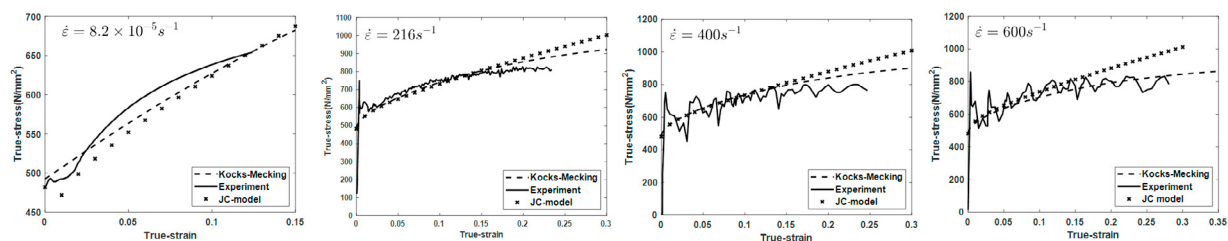


Fig. 5. Comparison of analytical results with the experiment at different strain rates.

The number of oscillations decreases with increasing strain rates and higher amplitudes. The test plots in Figs. 4a and 4b shows a reasonable agreement between the experimental and machine learning predicted stress-strain curves. This shows that machine learning algorithms can be used to predict stress-strain curves, but were limited by the number of available data, and hence the extensibility is not ascertained.

Table 3. Mechanical properties of X65 grade steel.

Mechanical Properties	Quasi-static	High strain rate
Youngs Modulus (MPa)	205-210	240-460
0.2% Proof strength (MPa)	486-500	640-688
Ultimate strength (MPa)	600	740-856
Elongation (%)	27	27-30

With a series of uniaxial tensile tests conducted, the JC ductile and failure model constants of X65 grade steel have been obtained at varying strain rates and room temperature. To mitigate the effects of oscillations on the results, some experimental techniques were adopted such as the use of EDM notched samples and fatigue pre-cracked samples. Comparisons were made with different types of testing including the impact drop weight testing and instrumented Charpy testing. Also, tensile tests on round and flat specimens were done for proper material characterisations at various strain rates. It is found that the yield strength at high strain rates and the ultimate strength of materials increase with strain rate. Other factors that affect the material properties were the geometry of the sample and the size and type of crack in the sample. The results from the different crack experiments showed that the EDM notched samples introduce oscillations unlike the fatigue pre-crack samples with smooth curves in Fig. 4c, and the EDM notched tend to be of higher peak than the pre-cracked samples which was thought by Kang et al. (2014) to be as a result of the crack tip variations between a blunt (EDM notched) and sharp crack (pre-cracked) where deformation sets in.

6. Conclusion

Different approaches have been applied to investigate the behaviour of X65 material at high strain rates including analytical, experimental, FEA and machine learning. The results show that various methods can be used to model dynamic testing. Being that the JC model has the limitation of predicting the parameters from first principles, hence thermostatistical model from analytical Equations 4 and 3 was established from known and assumed values. There is a good agreement with the experimental and JC model results. Predictions from machine learning algorithm correlates well with the experimental data. The obtained JC parameters were further applied to dynamic ABAQUS/explicit in the model presented in this work. The data-set used in training the machine learning algorithm to predict the stress-strain curve in this study was limited due to the high cost associated with the experiments. However, from the results shown, it is convincing that machine learning can predict the mechanical behaviour of materials.

Acknowledgements

This publication was made possible by the sponsorship and support of Lloyd's Register Foundation (LRF). The work was enabled through, and undertaken at, the National Structural Integrity Research Centre (NSIRC), a postgraduate engineering facility for industry-led research into structural integrity established and managed by TWI through a network of both national and international Universities.

Lloyd's Register Foundation helps to protect life and property by supporting engineering-related education, public engagement and the application of research. www.lrfoundation.org.uk

References

- F. F. Lavrentev, "The type of dislocation interaction as the factor determining work hardening," *Mater. Sci. Eng.* 46, 191–208 (1980). [https://doi.org/10.1016/0025-5416\(80\)90175-5](https://doi.org/10.1016/0025-5416(80)90175-5)
- Huang, M., Rivera-Díaz-del-Castillo, P. E., Bouaziz, O., van der Zwaag, S. (2009). A constitutive model for high strain rate deformation in FCC metals based on irreversible thermodynamics. *Mechanics of Materials*, 41(9), 982-988.
- Galindo-Nava, E. I., Rivera-Díaz-del-Castillo, P. E. J. (2012). Modelling plastic deformation in BCC metals: Dynamic recovery and cell formation effects. *Materials Science and Engineering: A*, 558, 641-648.
- Klopp, R. W., Clifton, R. J., & Shawki, T. G. (1985). Pressure-shear impact and the dynamic viscoplastic response of metals. *Mechanics of Materials*, 4(3-4), 375-385.
- F. Pedregosa, G. Varoquaux, A. Gramfort, V. Michel, B. Thirion, O. Grisel, M. Blondel, P. Prettenhofer, R. Weiss, V. Dubourg, J. Vanderplas, A. Pas-sos, D. Cournapeau, M. Brucher, M. Perrot, Edouard Duchesnay, Scikit-learn: Machine learning in python, *Journal of Machine Learning Research* 16012 (85) (2011) 2825–2830
- ISO 12135:2016 "Metallic materials. Unified method of test for the determination of quasistatic fracture toughness".
- Hirsch, E., & Plesek, J. (2006). A theoretical analysis of experimental results of shock wave loading of OFE copper relating the observed internal structure to the deformation mechanism. *International journal of impact engineering*, 32(8), 1339-1356.
- Kocks, U. F., Mecking, H. (2003). Physics and phenomenology of strain hardening: the FCC case. *Progress in materials science*, 48(3), 171-273.
- Johnson, G. R., and W. H. Cook. "In: Proceedings of Seventh International Symposium on Ballistics." *A Constitutive Model and Data for Metals Subjected to Large Strains, High Strain Rates and High Temperatures* (1983).
- Banerjee, A., Dhar, S., Acharyya, S., Datta, D., Nayak, N. (2015). Determination of Johnson cook material and failure model constants and numerical modelling of Charpy impact test of armour steel. *Materials Science and Engineering: A*, 640, 200-209.
- Kocks, U. F., & Mecking, H. (2003). Physics and phenomenology of strain hardening: the FCC case. *Progress in materials science*, 48(3), 171-273.
- BS EN ISO 6892-1:2019 "Metallic materials. Tensile testing. Method of test at room temperature".
- BS 7448-3:2005 "Fracture mechanics toughness tests. Method for determination of fracture toughness of metallic materials at rates of increase in stress intensity factor greater than 3.0 MPam^{0.5} s^{1/2}".
- BS ISO 26203-2:2011 Metallic materials. Tensile testing at high strain rates. Servo-hydraulic and other test systems.
- ASTM E1820 - 20 "Standard Test Method for Measurement of Fracture Toughness".
- Al-Mousawi, M. M., S. R. Reid, and W. F. Deans. "The use of the split Hopkinson pressure bar techniques in high strain rate materials testing." *Proceedings of the Institution of Mechanical Engineers, Part C: Journal of Mechanical Engineering Science* 211.4 (1997): 273-292.
- Kang, J., Shen, G., Liang, J., Gianetto, J. (2014). Influence of Constraint on J-resistance Curves for an X100 Pipe Steel. *Procedia materials science*, 3, 239-244.
- Kolsky, H. (1949). An investigation of the mechanical properties of materials at very high rates of loading. *Proceedings of the physical society. Section B*, 62(11), 676.